

# Trajectory of the August 7, 2010 Biwako Fireball Determined from Seismic Recordings

Masumi Yamada<sup>1</sup> and Jim Mori<sup>1</sup>

<sup>1</sup>*Disaster Prevention Research Institute, Kyoto University, Kyoto, Japan*

(Received ; Revised ; Accepted )

The Biwako fireball on August 7, 2010 produced a strong sonic boom throughout central Japan around 17:00 JST (UTC+9). There were many visual observations and reports of the sound in the Tokai and Kinki regions at that time. We estimated the trajectory of this fireball and location of its termination point by analyzing seismograms recorded on a dense local network. The isochrons of the arrival times are close to concentric circles, which suggest that the fireball disappeared due to fragmentation during entry. The fireball trajectory which explains the arrival times of the signal has a relatively high incident angle (55 degree relative to the horizon) and the source is thought to disappear at a height of 26 km east of Lake Biwa. The azimuthal angle and velocity of the fireball are difficult to determine uniquely from this dataset. We identified an event thought to be due to fragmentation, with a location 3 km ENE and 9 km higher than the termination point. This location is consistent with the trajectory determined from the signal arrival. Based on this trajectory model, the source of the signal spans a horizontal range of 26 to 70 km, and the altitude of the source producing the sonic boom is about 30 to 50 km.

**Key words:** 2010 Biwako fireball, estimation of trajectory, sonic boom, meteoroid, fragmentation

## 1. Introduction

The Lake Biwa (Biwako in Japanese) fireball on August 7, 2010 produced a strong sonic boom throughout central Japan around 17:00 JST (UTC+9). There were numerous reports of the track across

24 the sky and associated sounds in the region. A newspaper reported that the sonic boom was heard by  
25 local residents in the Tokai region (Aichi, Gifu, and Mie prefectures) and some people called emergency  
26 services to report the strong sound (asahi.com, 2010). Bright flashes were observed as far away as 250  
27 km from the termination point, as reported on an internet bulletin board (Japan Fireball Network, 1999).  
28 Local amateur astronomers have searched for the meteoroid which may have reached the ground, but  
29 nothing has been found so far (Onishi, 2010).

30 Past atmospheric trajectories of fireballs have been determined by visual recordings such as pho-  
31 tographs and movies (Brown et al., 1994, 2003), infrasound records (Brown et al., 2002; Le Pichon  
32 et al., 2002, 2008), and seismic records (e.g. Nagasawa, 1978; Nagasawa and Miura, 1987; Qamar,  
33 1995; Cevolani, 1994; Brown et al., 2002; Cates and Sturtevant, 2002; Le Pichon et al., 2002; Ishihara  
34 et al., 2003, 2004; Rydelek and Pujol, 2004; Pujol et al., 2005; Le Pichon et al., 2008). An object fly-  
35 ing at supersonic velocity produces a sonic boom, and the acoustic-to-seismic coupled signal is often  
36 recorded by seismic arrays. The airwave signal from this fireball was recorded on about 50 seismic  
37 stations in Japan (NIED, 2010). This is one of the few events with an airwave signal that is recorded by  
38 a dense seismic network (Walker et al., 2010). In this paper, we estimate the trajectory of the Biwako  
39 fireball and location of the termination point of the signal by analyzing the seismograms, and discuss  
40 the characteristic waveforms and mechanism of fireball fragmentation.

## 41 **2. Data**

### 42 **2.1 Seismic Data**

43 The Biwako fireball produced atmospheric sound waves that were recorded by Hi-net, F-net (both  
44 operated by the National Research Institute for Earth Science and Disaster Prevention), Japan Meteo-  
45 rological Agency high-sensitivity seismic network, and high-sensitivity seismic networks operated by  
46 Japanese universities (Okada et al., 2004). Those seismic networks currently have about 20 km spacing  
47 throughout Japan, and we identified shockwave signals from the fireball at 49 stations.

48 Since the onsets of the signal arrival are not very clear, we determined the arrival times as follows.  
49 First, a band-pass Butterworth filter with typical cutoff frequencies of 2 to 8 Hz was applied to each  
50 record to look at the frequency range of the infrasound signals. Since we used records from various type  
51 of sensors, we tried alternative high-pass Butterworth filters if the signal is not clear. The filtered records  
52 are shown in Figure 1. We used only vertical components for this analysis. The onset of the signal is  
53 determined by fitting a multi-variate locally stationary autoregressive (MLSAR) model (Takanami and  
54 Kitagawa, 1991). This technique is widely used to pick P-wave arrivals in the seismograms. The  
55 characteristics of the time series change over time due to the arrival of seismic waves. Therefore, the  
56 time series is divided into two segments, and the autoregressive model is fit to each segment. The log-  
57 likelihood of each multi-variate locally stationary autoregressive model is computed, and the Akaike  
58 information criterion (AIC) is used to determine the best onset time (Akaike, 1974). The onset of the  
59 signal is determined as a section that minimizes the AIC. Although this technique can identify the time  
60 that the characteristics of the waveforms have the most significant changes, there is a possibility that  
61 this onset time is contaminated by the air-coupled Rayleigh wave (Edwards et al., 2008). The arrival  
62 times determined by this method are marked as open triangles in Figure 1.

63 In contrast to some past observations (e.g. Cates and Sturtevant, 2002; Ishihara et al., 2003), the  
64 airwave signals from this event have unclear emergent onsets, long duration (10 - 40 seconds), and  
65 no distinct “N” shaped waves. The low apparent velocity ( $\sim 0.37$  km/sec) of the signals across  
66 the seismograph network indicates that the source of the signal is in the atmosphere, and is not an  
67 earthquake (see Figure 1).

68 Figure 2 shows the distribution of the arrival times of the shockwave. The first arrival was recorded  
69 at station DP.OHM (Ohmi-Hachiman) east of Lake Biwa, which indicates that the termination of the  
70 fireball is close to this station. The area where the signals are observed is within 170 km from this  
71 station. A notable feature of this fireball is that the isochron pattern consists of nearly concentric  
72 circles, not half-ellipses, as observed in most past studies (Cates and Sturtevant, 2002; Ishihara et al.,

2003).

## 2.2 Visual Observations

The Biwako fireball was observed by many people even in daylight around 17:00 local time, early evening in summer. Witnesses reported the locations and times of the sightings, durations of the flash, and directions of the fireball emergence on an internet bulletin board (Japan Fireball Network, 1999). Figure 3 shows the direction of the fireball observed by 34 witnesses. The fireball was observed from sites more than 250 km from the fireball trajectory. Although their reports are relatively rough (16-point compass directions, such as WSW, are usually used), the direction of the fireball is consistent in all reports. We can estimate that the explosive signal was produced near Lake Biwa from this figure. Some reports describe a fireball traveling with bright illumination twice to three times the size of the moon, and splitting into several parts before disappearing. Most of the witnesses reported that the white path of the meteor remained for a few minutes in the sky. The diamond symbols in Figure 3 represent the sites where sonic booms were observed (asahi.com, 2010). Here, a sonic boom is defined as a strong explosive sound with an impact, so sounds resembling distant thunder are excluded. Compared to the visual observations of the fireball, the observation of the sonic boom is in a more limited area.

## 3. Methods

We estimated the trajectory of the fireball and termination point of the signal using a method similar to Nagasawa and Miura (1987). This method assumes straight-ray theory and a constant velocity of sound. Since the arrival pattern of the signals are close to concentric circles, we assume that the fireball travelled toward the earth and terminated in the air (or at least stop producing atmospheric signals). A combination of line and point sources is considered to produce this arrival pattern. First, the fireball is moving through the air with high velocity producing nearly cylindrical ballistic waves, with an elliptical arrival pattern on the ground. Then, the fireball experiences a catastrophic fragmentation or disruption at a termination point, which causes arrivals in a pattern of concentric circles (Edwards et al., 2008).

97 The sites on the ground in the direction of the fireball trajectory record signals due to the fragmentation,  
 98 while sites on the ground perpendicular to the fireball trajectory record the ballistic wave and signals  
 99 from the fragmentation (see Figure 4).

100 Based on this assumption, we estimated the trajectory and termination point of the signal.

101 Estimated arrival times of the shockwave are represented with the following function (Nagasawa and  
 102 Miura, 1987). Here, we added an assumption that the object dissipates and the generation of the shock  
 103 wave stops at the termination point of the fireball, so extra parameters are added to the function.

$$t_{pred} = t_0 + 1/v(\sqrt{X^2 + Y^2}/\tan \beta - Z) \quad (1)$$

$$t_{pred} = t_0 + 1/c(\sqrt{X^2 + Y^2 + Z^2}) \quad (2)$$

$$\text{if } \begin{cases} Z \geq -\tan \beta \sqrt{X^2 + Y^2}, & \text{Eq. (1) (region A in Fig. 4)} \\ Z < -\tan \beta \sqrt{X^2 + Y^2}, & \text{Eq. (2) (region B in Fig. 4),} \end{cases}$$

104 where,

$$\beta = \arcsin(c/v)$$

$$\begin{pmatrix} X \\ Y \\ Z \end{pmatrix} = \begin{pmatrix} -\sin \gamma & \cos \gamma & 0 \\ -\cos \gamma \sin \theta & -\sin \gamma \sin \theta & \cos \theta \\ \cos \gamma \cos \theta & \sin \gamma \sin \theta & \sin \theta \end{pmatrix} \begin{pmatrix} x - x_0 \\ y - y_0 \\ z - z_0 \end{pmatrix}$$

105  $x_0, y_0, z_0$  : coordinates of the trajectory where the signal vanished

106  $t_0$ : time when the signal vanished

107  $\gamma$  : azimuth of the trajectory

108  $\theta$  : incident angle of the trajectory relative to the horizontal

109  $c$  : velocity of sound (0.312 km/s)

110  $v$  : velocity of the fireball (20 km/s)

111

112 The coordinate system used in this analysis is shown in Figure 4. The origin for the x,y,z coordinate  
 113 system is defined as longitude 136°E, latitude 35°N, and altitude 0 km, and the origin time is 17:00:00  
 114 JST. The speed of the sonic wave is assumed to be a constant with a value of 0.312 km/s taken from  
 115 Nagasawa and Miura (1987). The velocity of the fireball is a parameter which is difficult to constrain  
 116 because of the trade off with the time the signal vanishes, since the velocity of sound is slow with respect  
 117 to the observed duration of the signal assuming a range of reasonable fireball velocities (Ishihara et al.,  
 118 2003; Edwards et al., 2008). We computed a misfit surface for each parameter (see Figure 5) and the  
 119 result shows the velocity of the fireball is not sensitive to the rms residual of the arrival times, so a  
 120 fixed velocity of 20 km/s was used. (The misfit surface will be discussed in the next section.) Six  
 121 free parameters ( $x_0, y_0, z_0, t_0, \gamma, \theta$ ) that define the fireball trajectory are solved by minimizing the rms  
 122 residuals:

$$rms = \sqrt{\frac{1}{n-6} \sum_{i=1}^n (t_{pred,i} - t_{obs,i})^2}, \quad (3)$$

123 where  $n$  is the number of observations,  $t_{pred,i}$  is the predicted arrival time of the signal at the  $i$ th station,  
 124 and  $t_{obs,i}$  is the measured arrival time of the signal at the  $i$ th station. The 6 in the denominator is the  
 125 number of parameters to be estimated (Montgomery and Runger, 2003).

## 126 4. Analysis and Results

### 127 4.1 Estimation of the Trajectory

128 We performed a grid search to find the most probable set of parameters of the trajectory model. The  
 129 best fitting parameters of the trajectory that explain the arrival times of the shock wave are shown in  
 130 Table 1. Intervals of the grid search, search ranges, and confidence intervals of the parameters are also  
 131 included in the table. The isochrons of the arrival times based on this model are shown in Figure 2, and  
 132 the residuals of the arrival times are shown in Figure 1. The location of the termination point of the

133 signal is east of Lake Biwa, and the altitude of 26 km. The 95% confidence interval of each parameter is  
134 calculated by a bootstrap method with 100 replicates (Efron and Tibshirani, 1993; Walker et al., 2010).  
135 The uncertainties of the parameters  $x_0, y_0, z_0, t_0, \theta$  are small, since the arrival time of the shock wave  
136 is sensitive to these parameters. However, the azimuthal angle  $\gamma$  has a large confidence interval and  
137 is difficult to determine uniquely from this dataset, since most of the stations are inside the concentric  
138 isochrons and the azimuthal coverage of stations with distances greater than 100 km is poor.

## 139 4.2 Sensitivity Analysis

140 We computed misfit surfaces as a function of each parameter to check the sensitivity of the param-  
141 eters. The minimum of the rms residuals are computed as a function of two selected parameters (see  
142 Figure 5). The misfit surface for the horizontal location is smooth in both longitude and latitude, and  
143 has a single local minimum. Therefore, the solution easily converges to this minimum. The optimal  
144 time and altitude of the meteorite dissipation are both sensitive to the velocity of sound and difficult to  
145 resolve, but still a broad minimum exists in the surface. Note that these two parameters are also sensi-  
146 tive to the sound velocity. The perturbation of the parameters is about 10% if we change the velocity  
147 of the sound by 0.01 km/s. The azimuth of the trajectory is not very well determined by the dataset, as  
148 we have seen with the confidence interval. The velocity of the fireball is also significantly insensitive  
149 to the data, so we used a constant velocity for this analysis.

## 150 4.3 Interpretation of the Model

151 A mechanism to produce these concentric isochrons of the arrival times can be explained by an  
152 explosive fragmentation (Edwards et al., 2008). During a meteoroid entry, the object breaks up suddenly  
153 because of the increasingly large air pressure. A large amount of light is produced associated with the  
154 break up. Since these explosive fragmentation events are very brief and take place over small portions  
155 of the entire trajectory, they are approximated by a point source, and result in the concentric isochrons.

156 The non pulse-like waveforms can also be explained with this mechanism. The fragmentation may  
157 result in separation of the original body into several large fragments. The duration of the fragmentation

158 is largely unknown, however if fragmentation takes 0.5 second, the meteoroid can travel as far as 10  
159 km (assuming a constant velocity) during this time. This distance is comparable to a difference of  
160 32 seconds in arrival time of the waveforms. Therefore, the extremely long duration of the signal is  
161 not necessarily unreasonable (Walker et al., 2010). Edwards et al. (2008) explained that observations  
162 of an explosive point-source events tend to be diffuse, with no distinct arrival time, in contrast to  
163 the sharp onset of ballistic observations. Waveforms here are very similar to the waveforms of 2002  
164 Tagish lake fireball (Brown et al., 2002) and 1989 St. Helens fireball (Qamar, 1995), which both show  
165 concentric isochrons. Similar concentric isochrones were also observed in Arrowsmith et al. (2007) and  
166 Walker et al. (2010). Multipathing through the atmosphere might also complicate the character of the  
167 waveforms, however this is generally observed at distances greater than 200 km (Walker et al., 2010)  
168 which is not the range of the data in this study.

#### 169 **4.4 Height of the Source**

170 The airwave signal was observed by seismometers as far away as 150 km, and the bright flashes were  
171 observed as far away as 250 km from the termination point (Japan Fireball Network, 1999). We try to  
172 estimate the altitude of the termination point from the trajectory model. Figure 4 shows a schematic  
173 diagram of the fireball trajectory and meteor-generated atmospheric waves. If the source dissipates  
174 at 26 km altitude, the ballistic wave due to the object flying at supersonic speed cannot be observed  
175 within 40 km from the epicenter. The signal observed in this near-source region is not impulsive due  
176 to the fragmentation. Assuming a line source, the height of a source which is observable 150 km  
177 from the center of the arrival time pattern must be at least 70 km high. Therefore, the source of the  
178 signal is inferred to be between 26 and 70 km, and could be higher if there is strong attenuation in the  
179 atmosphere. Reports of the sonic boom concentrate in the Tokai region, about 50-100 km from the  
180 center of the arrival time pattern. The altitude of the source corresponding to this signal is about 30  
181 to 50 km high. This height is consistent with past observations; 22 to 34 km for the 2000 Moravka  
182 fireball and 34 to 87 km for the 2003 Kanto fireball (Pujol et al., 2006). For the Biwako fireball,

183 we located the two fragmentation events at heights of 26 and 35 km. It has been suggested that the  
 184 height of fragmentation is where the aerodynamic pressure exceeds the material strength. Cevolani  
 185 (1994) calculated the critical heights of the first fragmentation for meteoroids with different values of  
 186 the material strength. According to the table, the critical height is 45.5 to 56.5 km for dustballs, 14 to  
 187 38 km for stony chondrites, and 3 to 14 km for metal bodies, at velocities of 15 to 30 km/s. From these  
 188 values, we speculate that the material of this fireball may be a stony chondrite.

## 189 5. Different Models

### 190 5.1 Point Source Model

191 We also examined a simple point source model to try to explain the same dataset. If the observed  
 192 arrivals are produced by the terminal explosion in a very short time frame, the arrival time pattern  
 193 should be explained by a simple point source model. We used the same dataset as in section 2, and the  
 194 same method as in section 3 except the velocity of the fireball, and the incident angle and azimuth of  
 195 the trajectory are now set to be zero. The estimated arrival times are computed from equation (1). The  
 196 most probable parameter set from the grid search is shown in Table 2. We compared the two models  
 197 (point source + line source model and simple point source model) with an F-test. The null hypothesis  
 198 is the case where the two models predict the dataset equally well. The F statistic is given by

$$F = \left( \frac{\text{RSS}_1 - \text{RSS}_2}{p_2 - p_1} \right) / \left( \frac{\text{RSS}_2}{n - p_2} \right) = 48.11 \quad (4)$$

199 where  $\text{RSS}_i$  is the residual sum of squares of model  $i$ ,  $p_i$  is the number of parameters of model  $i$ , and  $n$   
 200 is the number of observations. From the F distribution table, the F value with  $(p_2 - p_1, n - p_2)$  degrees  
 201 of freedom at a 5% significance level is 3.21. Therefore, the null hypothesis has a low probability of  
 202 being accepted, and the more complicated model provides a significantly better fit to the data.

### 203 5.2 Back Projection Method

204 Since we used times of the onset of the signal for the location estimation, these arrival times  
 205 correspond to the location of the end of terminal explosion. We applied a back projection method

to the waveforms in order to find the location where the fireball produced the largest energy.

The waveforms used here are the same as the dataset in section 2. Since the correlation distance of infrasound at 0.5 to 5 Hz is only several kilometers (Walker et al., 2010), we used envelopes of the waveforms. The data are processed as follows; envelopes of the waveforms are formed using the maximum absolute value of the waveforms over one second windows. To remove the effect of stationary noise, the mean over a 10 minutes duration is removed. Then, the maximum amplitude of the signal is normalized to one to regularize the amplitude of the envelopes.

The back projection method used here is similar to the reverse time migration technique in Walker et al. (2010). However, the stack of the waveform amplitudes ( $Q$ ) is defined as a function of longitude, latitude, altitude, and time in our analysis. The maximum for every second  $t$  is defined as  $Q_t$ . The weighting is set to be one since our station distribution is not greatly skewed. The search range is the same as shown in Table 2. Figure 6 shows  $Q_t$  as a function of  $t$ . The  $Q_t$  has a local maxima between 55 and 60 seconds, the optimal parameters at those times are shown in Table 3.

The computed location of the source producing the largest energy is located around 136.105E and 36.165N, about 3 km ENE and 9 km higher than the termination point. This location is consistent with the trajectory determined from the arrivals at the seismic stations, since the path from the source producing the largest energy to the terminal point is similar to the calculated trajectory. Because the source of the largest energy is at a higher altitude than the termination burst, it was recorded a few tens of seconds later at some stations.

## 6. Conclusions

We estimated the trajectory of the August 7, 2010 Biwako fireball and location of its termination point from arrivals at seismic stations. The isochrons of the arrival times are nearly concentric circles, which suggest that the fireball dissipated due to fragmentation during entry. The fireball trajectory which explains the arrival times of the signal has a relatively high incident angle (55 degree) and the

230 source is thought to disappear at a height of 26 km east of Lake Biwa. The azimuthal angle and velocity  
231 of the fireball are difficult to determine uniquely from this dataset. We identified an event thought to  
232 be due to fragmentation, with a location 3 km ENE and 9 km higher than the termination point. This  
233 location is consistent with the trajectory determined from the arrival time data. Based on this trajectory  
234 model, the location of the source of the signal spans a range of 26 to 70 km, and the altitude of the  
235 source producing the sonic boom is about 30 to 50 km.

236 **Acknowledgments.** The authors thank Yoshihisa Iio of Kyoto University for providing data observed west of Lake Biwa. We  
237 acknowledge the National Research Institute for Earth Science and Disaster Prevention (NIED) and Japan Meteorological Agency (JMA)  
238 for the use of the seismic data. This research was supported by the Program for Improvement of Research Environment for Young  
239 Researchers from Special Coordination Funds for Promoting Science and Technology (SCF) commissioned by the Ministry of Education,  
240 Culture, Sports, Science and Technology (MEXT) of Japan.

## 241 References

- 242
- 243 Akaike, H. (1974). A new look at the statistical model identification. *IEEE Transactions on Automatic Control*, **19**, 716–723.
- 244 Arrowsmith, S., Drob, D., Hedlin, M., and Edwards, W. (2007). A joint seismic and acoustic study of the Washington state bolide: Observations and  
245 modeling. *Journal of Geophysical Research*, **112**, D09304.
- 246 asahi.com (2010). Reported detonation in the wide area in Tokai region, no damage reported, <http://www.asahi.com/special/playback/ngy201008070006.html>.  
247 Accessed 20 November 2010, (in Japanese).
- 248 Brown, P., Ceplecha, Z., Hawkes, R., Wetherill, G., Beech, M., and Mossman, K. (1994). The orbit and atmospheric trajectory of the Peekskill meteorite  
249 from video records. *Nature*, **367**, 624–625.
- 250 Brown, P., Kalenda, P., Revelle, D., and Borovicka, J. (2003). The Moravka meteorite fall: 2. interpretation of infrasonic and seismic data. *Meteoritics &*  
251 *Planetary Science*, **38**, 989–1003.
- 252 Brown, P., Revelle, D., Tagliaferri, E., and Hildebrand, A. (2002). An entry model for the Tagish Lake fireball using seismic, satellite and infrasound  
253 records. *Meteoritics and Planetary Science*, **37**, 661–676.
- 254 Cates, J. and Sturtevant, B. (2002). Seismic detection of sonic booms. *The Journal of the Acoustical Society of America*, **111**, 614–628.
- 255 Cevolani, G. (1994). The explosion of the bolide over Lugo di Romagna (Italy) on 19 January 1993. *Planetary and Space Science*, **42**, 767–775.
- 256 Edwards, W., Eaton, D., and Brown, P. (2008). Seismic observations of meteors: Coupling theory and observations. *Reviews of Geophysics*, **46**, RG4007.
- 257 Efron, B. and Tibshirani, R. (1993). An introduction to the bootstrap. Chapman & Hall.
- 258 Ishihara, Y., Furumoto, M., and Shin'ichi Sakai, S. (2004). The 2003 Kanto large bolide's trajectory determined from shockwaves recorded by a seismic  
259 network and images taken by a video camera. *Geophysical Research Letters*, **31**, L14702.
- 260 Ishihara, Y., Tsukada, S., Sakai, S., Hiramatsu, Y., and Furumoto, M. (2003). The 1998 Miyako fireball's trajectory determined from shock wave records  
261 of a dense seismic array. *Earth, Planets and Space*, **55**, 9–12.
- 262 Japan Fireball Network (1999). Bulletin board of the Japan fireball network, <http://www3.cnet.ne.jp/c-shimo/index.html>. Accessed 20 November 2010,  
263 (in Japanese).
- 264 Le Pichon, A., Antier, K., Cansi, Y., Hernandez, B., Minaya, E., Burgoa, B., Drob, D., Evers, L., and Vaubaillon, J. (2008). Evidence for a meteoritic origin

Table 1. The most probable parameters which determine the trajectory of the fireball.

Parameters	Optimal solution	Search Range	Grid interval	Confidence Interval
Longitude (deg.)	136.073	136.0-136.2	0.001	136.055-136.090
Latitude (deg.)	36.149	35.0-35.2	0.001	35.140-35.160
Height (km)	26	0-50	1	22-30
Time (sec)	58	50-80	1	53-65
Incident ang. (deg.)	55	30-90	1	51-60
Azimuth (deg.)	32	0-180	1	16-63
RMS (sec)	6.86	-	-	-

- 265 of the September 15, 2007, Carancas crater. *Meteoritics & Planetary Science*, **43**, 1797–1809.
- 266 Le Pichon, A., Guérin, J., Blanc, E., and Reymond, D. (2002). Trail in the atmosphere of the 29 December 2000 meteor as recorded in Tahiti: Characteristics  
267 and trajectory reconstitution. *Journal of Geophysical Research*, **107**, 4709.
- 268 Montgomery, D. and Runger, G. (2003). *Applied Statistics and Probability for Engineers, 3rd edition*. Wiley and Sons.
- 269 Nagasawa, K. (1978). An analysis of sonic boom from a great fireball on May 10, 1977, recorded on seismographs of volcano observatories. *Bull.*  
270 *Earthquake Res. Inst. Univ. Tokyo*, **53**, 271–280.
- 271 Nagasawa, K. and Miura, K. (1987). Aerial path determination of a great fireball from sonic boom records on seismographs. *Bull. Earthquake Res. Inst.*  
272 *Univ. Tokyo*, **62**, 579–588.
- 273 NIED (2010). The signal from the August 7, 2010 fireball observed by Hinet, NIED, <http://www.hinet.bosai.go.jp/topics/fball100807/>. Accessed 20  
274 November 2010, (in Japanese).
- 275 Okada, Y., Kasahara, K., Hori, S., Obara, K., Sekiguchi, S., Fujiwara, H., and Yamamoto, A. (2004). Recent progress of seismic observation networks in  
276 Japan - Hi-net, F-net, K-NET and KiK-net. *Earth, Planets and Space*, **56**, 15–28.
- 277 Onishi, M. (2010). Search for a meteor which might have reached around Biwako. *Kyoto Shimbun*, November 7, 2010. local news section, (in Japanese).
- 278 Pujol, J., Rydelek, P., and Bohlen, T. (2005). Determination of the trajectory of a fireball using seismic network data. *Bulletin of the Seismological Society*  
279 *of America*, **95**, 1495–1509.
- 280 Pujol, J., Rydelek, P., and Ishihara, Y. (2006). Analytical and graphical determination of the trajectory of a fireball using seismic data. *Planetary and Space*  
281 *Science*, **54**, 78–86.
- 282 Qamar, A. (1995). Space shuttle and meteoroid - tracking supersonic objects in the atmosphere with seismographs. *Seismological Research Letters*, **66**,  
283 6–12.
- 284 Rydelek, P. and Pujol, J. (2004). Real-time seismic warning with a two-station subarray. *Bulletin of the Seismological Society of America*, **94**, 1546–1550.
- 285 Takanami, T. and Kitagawa, G. (1991). Estimation of the arrival times of seismic waves by multivariate time series model. *Annals of the Institute of*  
286 *Statistical Mathematics*, **43**, 407–433.
- 287 Walker, K., Hedlin, M., de Groot-Hedlin, C., Vergoz, J., Le Pichon, A., and Drob, D. (2010). Source location of the 19 February 2008 Oregon bolide using  
288 seismic networks and infrasound arrays. *Journal of Geophysical Research*, **115**, B12329.

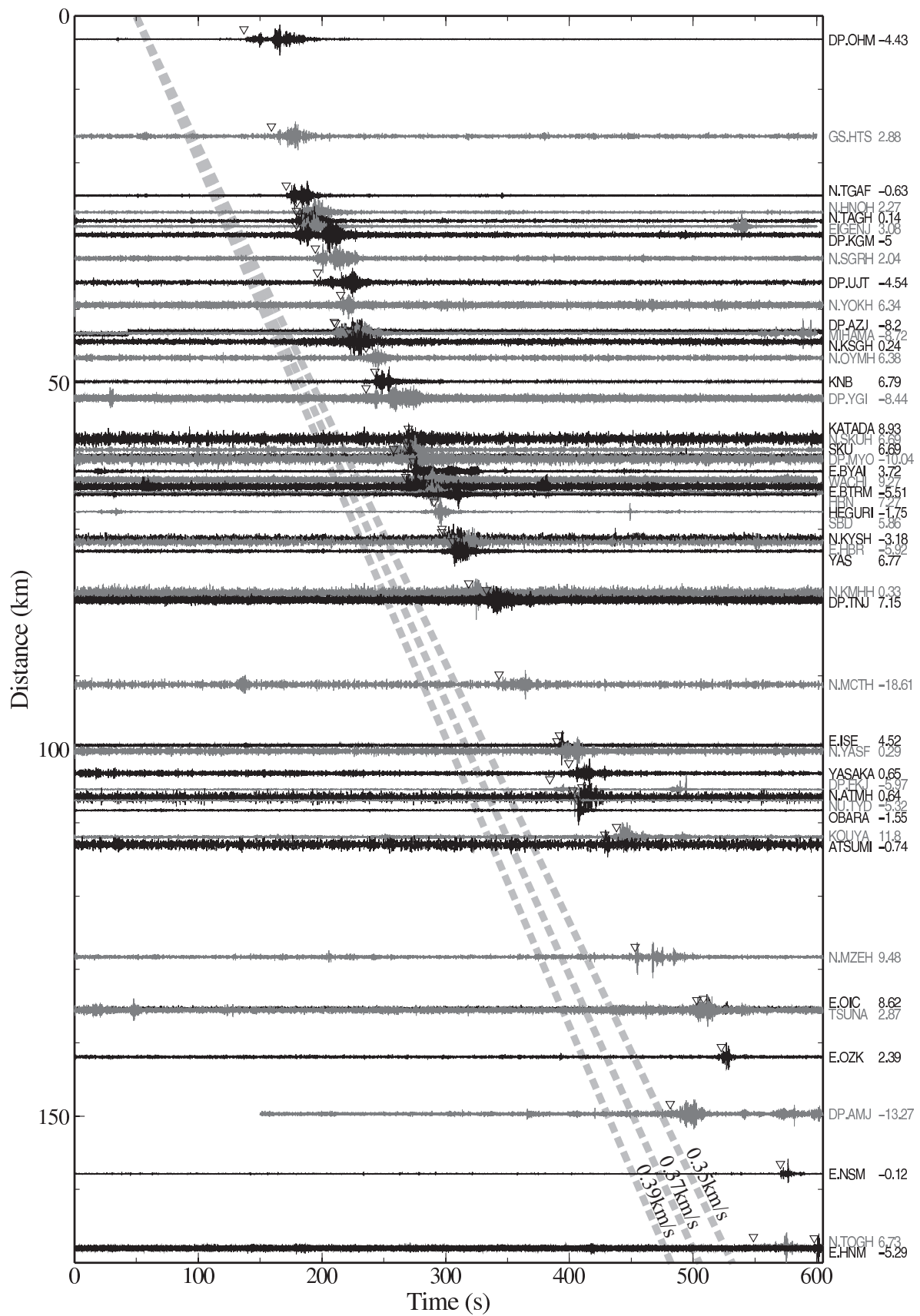


Fig. 1. Waveforms ordered as a function of distance from the termination point. The open triangles show the observed arrival times. The station code and residual of the arrival time ( $t_{pred} - t_{obs}$ ) are added on the right side. Alternate seismograms are shown in black and gray for clarity.

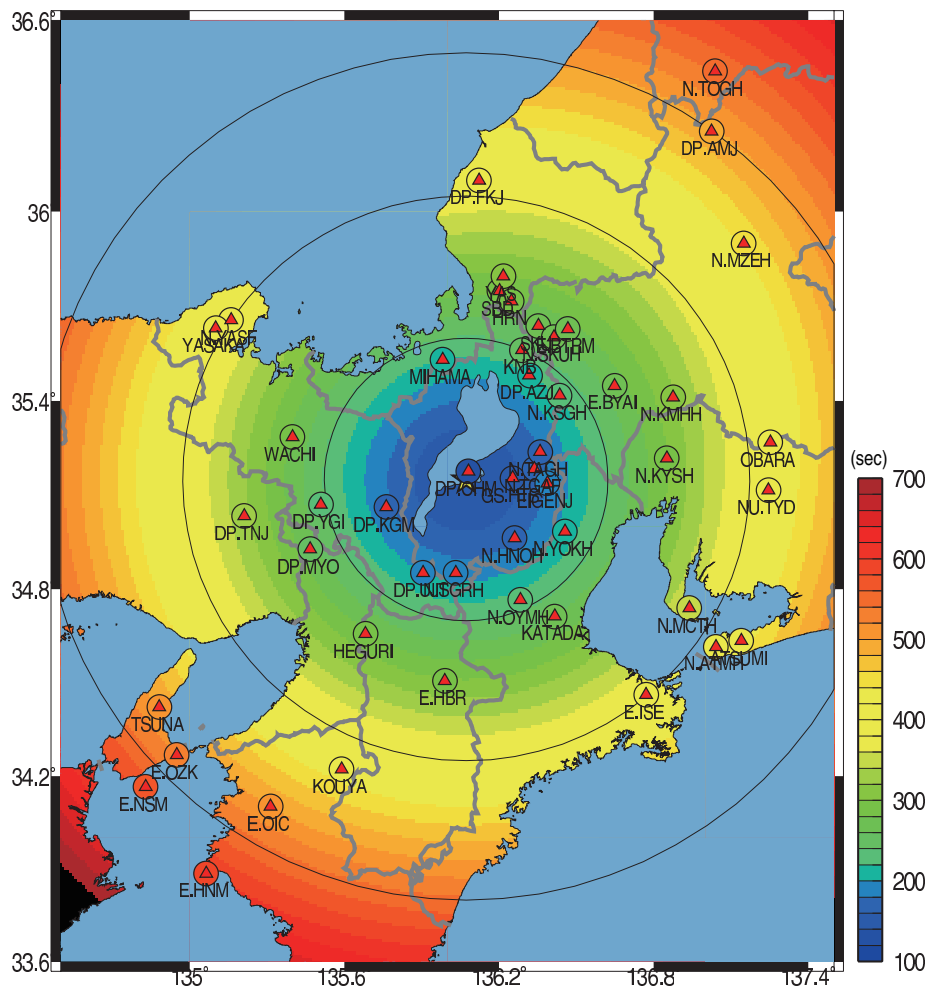


Fig. 2. Observed arrival times of the shockwave (color of the small circle at stations) and predicted arrival times of the shockwave based on the trajectory model (color contours). The large circles indicate distances of 50, 100, and 150 km from the estimated termination point of the signal.

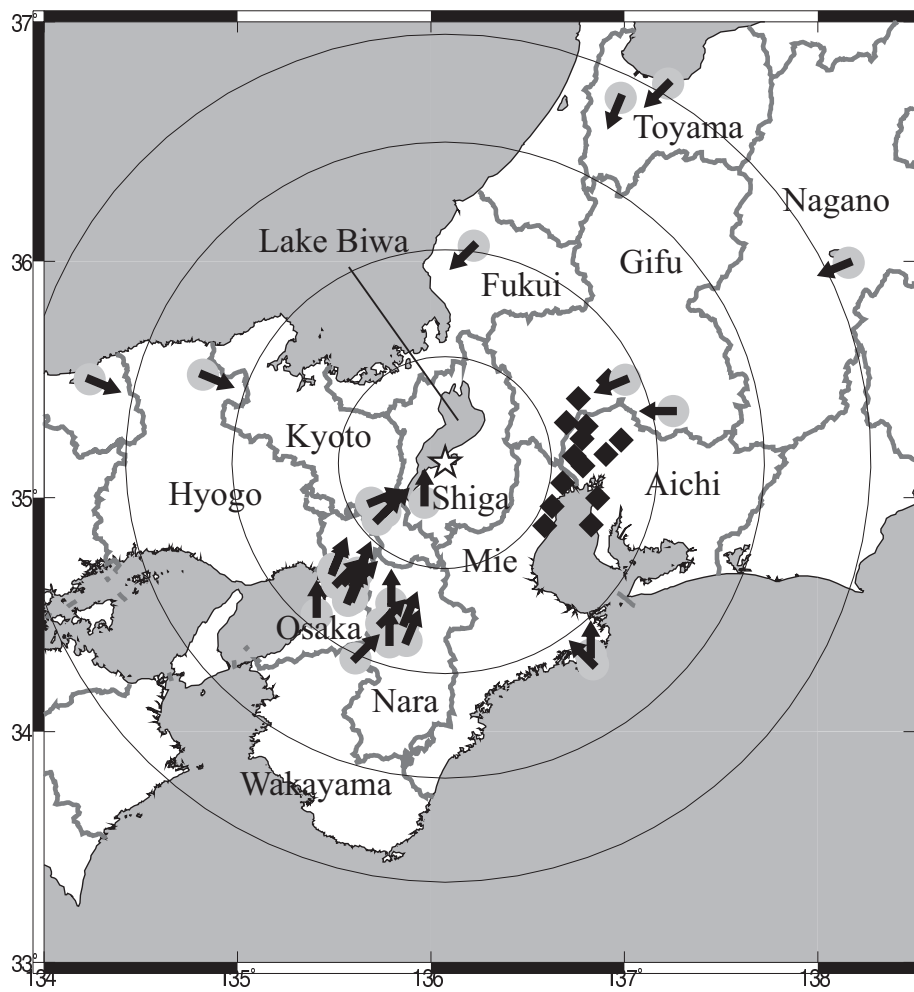


Fig. 3. Directions of the fireball observed by 34 witnesses. The diamond symbols show the sites where sonic booms were heard. Star shows the termination point of the signal. The large circles show distances of 50, 100, 150, and 200 km from the estimated termination point of the signal.

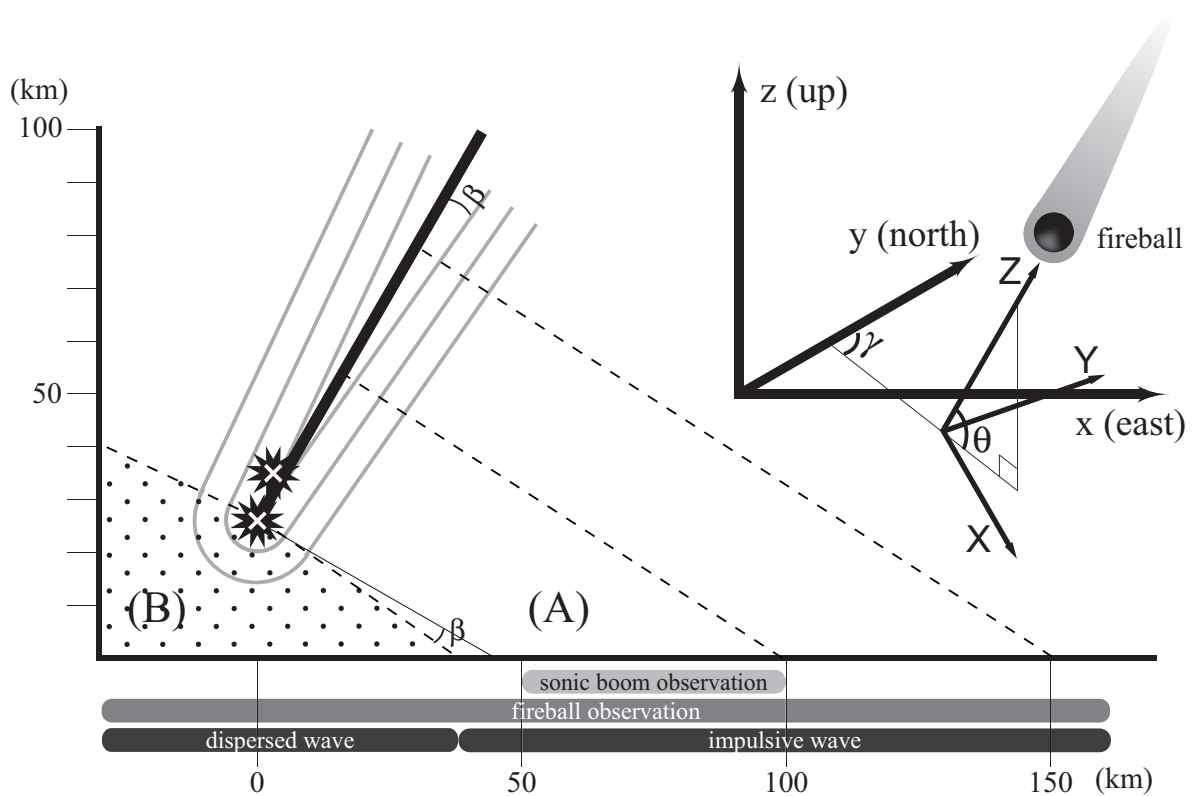


Fig. 4. Schematic diagram of meteor-generated atmospheric waves. In region A, the signal is explained by a line source, and in region B by a point source.

Coordinate systems used in the analysis are shown in right-hand side. Origins for the  $x, y, z$  coordinate system are longitude 136E, latitude 35N, and 0 km altitude, respectively. See the text for details.

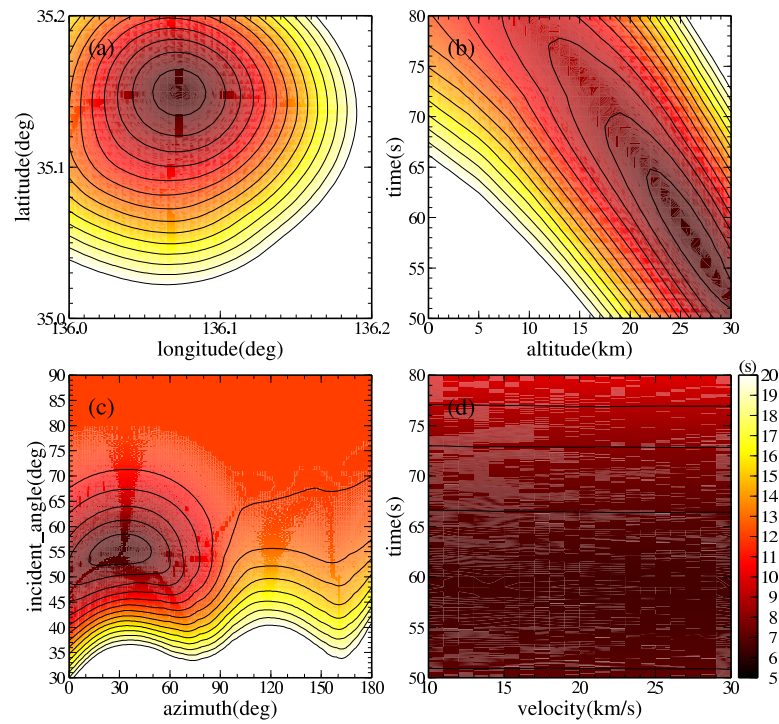


Fig. 5. Misfit surface for parameters. The rms residuals are computed as function of two out of six of the parameters to see the trade-off between parameters.

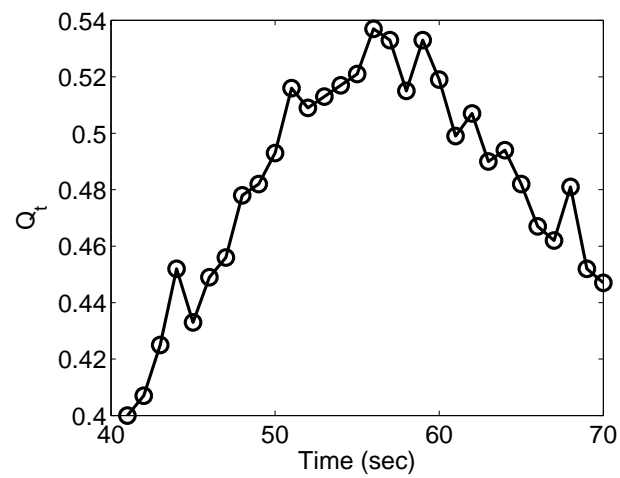


Fig. 6. Amplitudes of the stack of the waveforms from the back projection analysis, as a function of time.

Table 2. The most probable parameters which determine the trajectory of the fireball from point source model.

Parameters	Optimal solution	Search Range	Grid interval
Longitude (deg.)	136.086	136.0-136.2	0.001
Latitude (deg.)	36.172	35.0-35.2	0.001
Height (km)	33	0-50	1
Time (sec)	45	40-70	1
RMS (sec)	12.07	-	-

Table 3. The most probable parameters which determine the trajectory of the fireball from back projection.

Parameters	55sec	56sec	57sec	58sec	59sec	60sec
Longitude (deg.)	136.102	136.091	136.108	136.104	136.109	136.115
Latitude (deg.)	35.169	35.168	35.162	35.168	35.163	35.163
Height (km)	36	35	36	34	35	35
$Q_t$	0.521	0.537	0.533	0.515	0.533	0.519